Strain-Induced Pseudoheterostructure Nanowires Confining Carriers at Room Temperature with Nanoscale-Tunable Band Profiles

Donguk Nam,[†] David S. Sukhdeo,[†] Ju-Hyung Kang,[‡] Jan Petykiewicz,[†] Jae Hyung Lee,[†] Woo Shik Jung,[†] Jelena Vučković,[†] Mark L. Brongersma,*[,‡] and Krishna C. Saraswat*[,†]

[†]Department of Electrical Engineering and [‡]Department of Materials Science and Engineering, Stanford University, Stanford, California 94305, United States

S Supporting Information

ABSTRACT: Semiconductor heterostructures play a vital role in photonics and electronics. They are typically realized by growing layers of different materials, complicating fabrication and limiting the number of unique heterojunctions on a wafer. In this Letter, we present single-material nanowires which behave exactly like traditional heterostructures. These pseudo-heterostructures have electronic band profiles that are custom-designed at the nanoscale by strain engineering. Since the band profile depends only on the nanowire geometry with this approach, arbitrary band profiles can be individually tailored at the nanoscale using existing nanolithography. We report the first experimental observations of spatially confined, greatly enhanced (>200×), and wavelength-shifted (>500 nm) emission from strain-induced potential wells that facilitate effective carrier collection at room temperature. This work represents a fundamentally new paradigm for creating nanoscale devices with full heterostructure behavior in photonics and electronics.

KEYWORDS: Strain, pseudoheterostructure, heterostructure, nanowire, photoluminescence, germanium
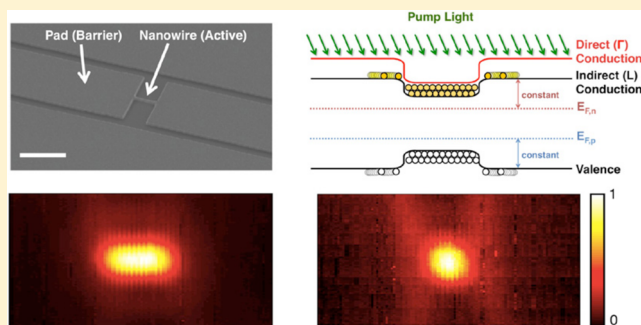
Since their introduction over half a century ago, semiconductor heterostructures have revolutionized electronic and photonic devices, in particular diode lasers and solar cells.[1−5] Using a so-called "double heterostructure" wherein a narrow band gap region is sandwiched between two wide band gap regions, carriers can readily be confined in the narrow band gap region. This carrier confinement is especially vital to efficient laser operation.[6,7] Until now, however, room temperature heterostructure behavior was only achievable by stacking layers of different semiconductor materials together with substantial band offsets. For example, band offsets well in excess of the thermal energy kT at room temperature (∼26 meV) are required to confine or trap carriers. Heteroepitaxy is costly due to the associated chemical vapor deposition (CVD) or molecular beam epitaxy (MBE) processes and often further complicated by large lattice mismatches and/or incompatible thermal budgets for different semiconductors.[8] Moreover, since a different process step is required for each new material, only a small number of unique heterojunctions can be fabricated on a single wafer. All of these problems can be avoided if one can create heterostructures within a single material by locally modifying the material's band gap. Strain engineering is a well-established technique to modify the electronic band gap of virtually all semiconductors.[9] The lattice constant of a crystalline semiconductor increases with tensile strain, thereby reducing its electronic band gap.[10] Previously, researchers have shown spatial band gap modulation by mechanically bending

nanostructures[11−13] and by depositing stressor layers.[14,15] However, these methods have thus far been limited by either practicality or design flexibility for realizing heterostructure behavior within a single material, and no meaningful optical or electronic functions were experimentally demonstrated at room temperature.

Here, we present the first experimental observation of room temperature carrier confinement within germanium (Ge) nanowires by creating strain-induced potential wells (>50 meV). By tuning the strain profiles within Ge nanowires, custom-designed electronic band profiles at the nanoscale were realized, and arbitrary heterostructure profiles within nanowires of a single material were created. This single-material nanowire with full heterostructure behavior is termed pseudo-heterostructure in this work. An effective carrier collection within each strain-induced potential well increases the local carrier concentration significantly in an ultracompact area, resulting in spatially confined and enhanced light emission. The emission wavelength is also red-shifted due the local band gap reduction in the tensile-strained nanowires. In this Letter, we demonstrate the spatially confined (Figure 3), enhanced (Figure 4a), and red-shifted (inset to Figure 4a) emission
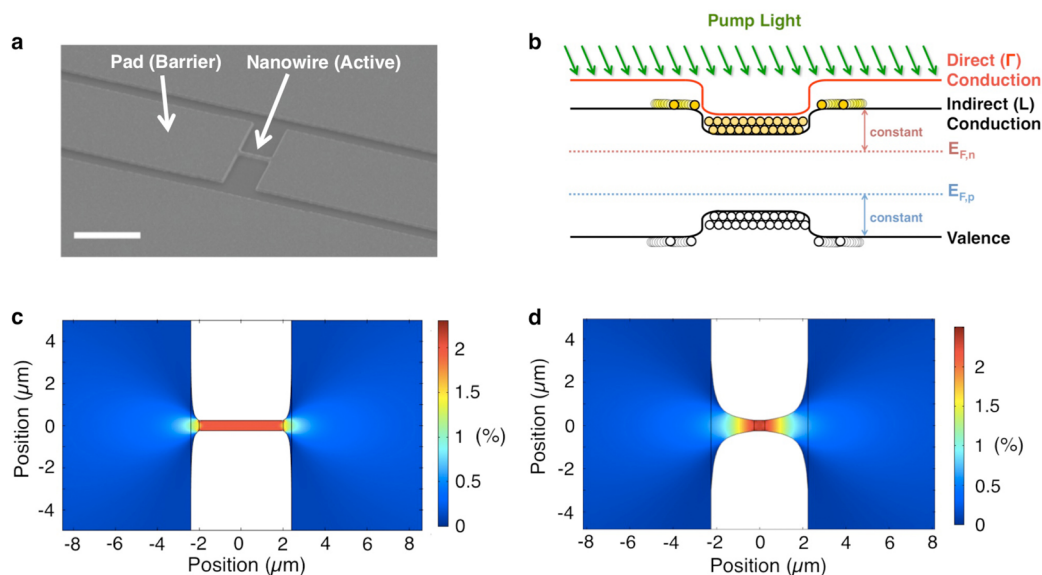
Figure 1. Strain-induced pseudoheterostructure nanowires. (a) SEM image of a fabricated and fully suspended structure. Scale bar, 5 μm. (b) Schematic of the energy band diagram along the center of the structure showing a strain-induced potential well and captured carriers. Quasi-Fermi levels for electrons and holes are also indicated. (c) Finite-element COMSOL simulation for an s-DH. (d) Finite-element COMSOL simulation for an s-GDH.

and quantitatively compare these results to our theoretical model.

Figure 1a shows a scanning electron micrograph (SEM) of a typical pseudoheterostructure nanowire. It was realized by extending upon a strain concentration technique used for Si nanowires,[16] which allowed us to induce localized strains greater than 2% in the nanowire—termed the active region—with the adjoining pad regions—also termed barriers—under only ∼0.1% strain. The fabrication process consists of a combination of electron-beam lithography on a Ge-on-insulator (GOI) wafer and dry and wet etching, as described in the Methods section in the Supporting Information. When the patterned Ge layer with pre-existing 0.2% biaxial tensile strain is suspended by underetching, the strain in the transverse direction is relaxed everywhere, while an interesting phenomenon occurs for the remaining longitudinal uniaxial strain. Along this axis, the barrier regions relax, shrink in size, and pull apart the central active region. This causes significant uniaxial strain concentration in the active region, while the strain in the barrier is reduced. By changing the length of the suspended barrier regions with fixed active region geometry, various degrees of uniaxial strain along the [100] direction can be selectively induced in the active region (see Figure S1 in the Supporting Information for SEM images of pseudoheterostructures with various active region strain levels). While the dimension of the active region was kept constant throughout this experiment, any arbitrary geometry of the active region can be used for creating pseudoheterostructure nanowires since the strain level depends only on geometrical factors, such as the length and width ratios of the barrier and the active regions.[16] Because a large strain within the active region greatly reduces the electronic band gap and enables electron and hole confinement within deep potential wells (>50 meV for both electrons and holes at ∼2.3% strain), this structure represents the first realization of double heterostructure behavior, that is capable of confining carriers at room temperature, within a single material. Figure 1b shows the electronic band profile along the active region of the nanowire

pseudo double heterostructure. This band profile as well as the energy locations of the quasi-Fermi levels will play a central role in explaining the observed optical behavior of the pseudoheterostructure nanowires. We will later quantify how photo-excited carriers in the barrier region diffuse into and are captured within the strain-induced potential well. This significantly increases the local carrier concentration within the active region, resulting in a spatially confined, enhanced, and wavelength-shifted light emission from the strain-induced potential well.

Figure 1c and d shows finite-element COMSOL simulations conducted to predict strain distributions in two pseudo-heterostructure nanowires with unique, engineered strain profiles: (1) a strain-induced double heterostructure (s-DH) and (2) a strain-induced graded double heterostructure (s-GDH). While the s-DH shows a relatively abrupt change in strain at the interface between the barrier and the active region, the strain in the s-GDH increases gradually toward the center of the active region. Since the strain in the active region is approximately inversely proportional to the width at every point along the active region, we intentionally taper the width of the active region hyperbolically with position to create the s-GDH with an approximately linear strain gradient. Unlike the conventional way to make heterostructures, this method clearly presents extreme design flexibility to engineer heterostructure behavior with nanoscale-tunable electronic band profiles that may be hard to achieve via heteroepitaxy (see Figure S2 in the Supporting Information for more pseudoheterostructure nano-wire designs).

Figure 2a and b shows SEM images of the s-DH and the s-GDH, respectively. The width of the active region in the s-DH is kept constant (∼500 nm), while the s-GDH features a hyperbolically tapered width along the active region. Figure 2c and d shows the 2D strain distributions of the two pseudoheterostructure nanowires measured by Raman spectroscopy (see Methods section in the Supporting Information). In the s-DH, the strain abruptly increases in the active region and remains constant along it. On the other hand, the strain in
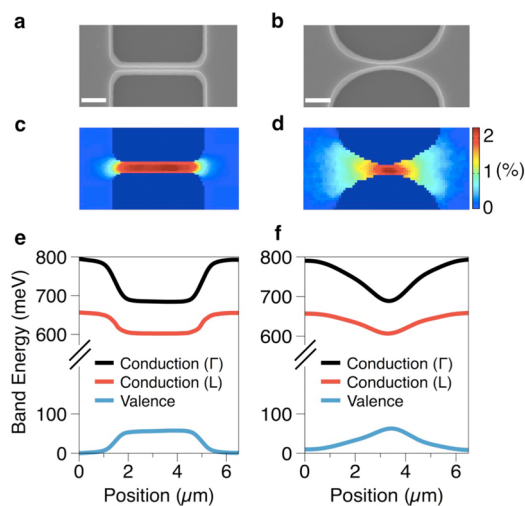
Figure 2. Pseudoheterostructure nanowires with custom-designed band profiles at the nanoscale. (a) SEM image of a fabricated s-DH. Scale bar, 1 μm. (b) SEM image of a fabricated s-GDH. Scale bar, 1 μm. (c) 2D Raman strain mapping of an s-DH. (d) 2D Raman strain mapping of an s-GDH. The units of the color bar represent uniaxial strain along the [100] direction. (e) Calculated band diagram along the active region of the s-DH. (f) Calculated band diagram along the active region of the s-GDH.

the s-GDH gradually changes toward the center of the active region. As shown in the measured Raman shift spectrum in Figure S3a, the strain in the barrier is slightly relaxed from 0.2% down to 0.1%, while the strain in the active region of the s-DH is significantly increased to 2.25%. The maximum strain at the center of the s-GDH is 2.30%. Figure 2e and f shows the calculated spatial dependence of the band edges along the active region. The measured strain values were converted into the band offsets using deformation potential theory,[17] and a 1D finite element-method (FEM) Poisson solver was used to calculate the band diagram of the pseudoheterostructure nanowires including band-bending effects as explained in the Supporting Information. The s-DH presents a square-like potential well, whereas the s-GDH shows a graded potential well. With a clear type-I band offset in these structures and well-

depths considerably exceeding kT, excited carriers (both electrons and holes) in the barriers will diffuse into and be captured within the potential well of the active region.

To demonstrate the ability to confine carriers within the potential well of the active region, microphotoluminescence (micro-PL) measurements were conducted. A Gaussian excitation laser spot of approximately 15 μm in diameter was used to ensure a relatively constant excitation over the entire area of interest (see Methods in the Supporting Information). Figure 3a and b shows optical images of the s-DH (with 2.25% strain along the active region) and the s-GDH (with 2.30% strain at the center of the active region). Figure 3c and d shows the corresponding spatial photoluminescence (PL) maps for the s-DH and the s-GDH, respectively. Cross-sectional PL intensity variations along the active regions (along the broken white lines) are presented below.

In the 2.25% strained s-DH, the carrier confinement effect significantly increases the carrier concentration in the active region, thereby showing much greater PL emission from the active region than from the barrier (Figure 3c). Because the depth of the potential well in the s-DH is approximately constant along the active region, the carriers captured within the potential well are uniformly distributed over the whole active region, resulting in enhanced emission from the entire width of the active region. It should be noted that, without the strong carrier confinement effect from the strain-induced potential well, the emission from the nanowire is weaker than the emission from its barrier because of the greater surface recombination in the nanowire (see Figure S4 in the Supporting Information). In the s-GDH, on the other hand, the gradients in the conduction and valence band edges force the electrons and holes into the center of the active region by setting up quasi-electric fields.[18] Therefore, the carrier concentration is greatly increased only at the center of the active region, leading to enhanced emission in the narrowest region (Figure 3d). We note that these strain-induced pseudoheterostructures are capable of concentrating carriers in any desired locations along the nanowire. Tailoring the carrier concentrations within a compact area would be particularly beneficial for electrically injected semiconductor lasers. For instance, semiconductor lasers often use composi-
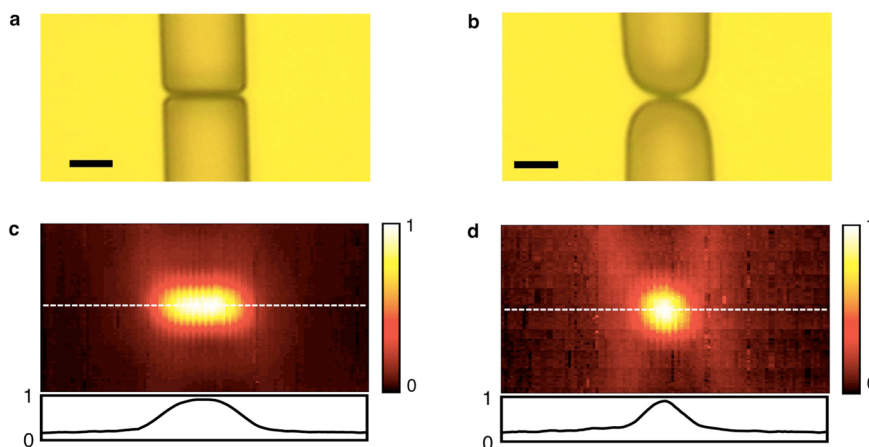

Figure 3. Spatially confined light emission from the strain-induced potential wells. (a) Optical micrograph of an s-DH. Scale bar, 2 μm. (b) Optical micrograph of an s-GDH. Scale bar, 2 μm. (c) 2D photoluminescence (PL) map of an s-DH with 2.25% strain in the active region, showing bright emission along the active region. (d) 2D PL map of an s-GDH with 2.30% strain at the center of the active region, showing concentrated, bright emission at the center of the active region. The units of the color bar represent the normalized PL intensity. Insets in Figure 2c and d represent cross-sectional PL intensity variations along the active regions (along the white broken lines).

tionally graded heterostructures to lower the lasing threshold by locally increasing the carrier density.[19,20]

To further verify the proper operation of these pseudo-heterostructure nanowires, we also analyzed how the spectral properties and intensity of the emission depend on the applied strain. Figure 4a shows PL spectra from s-DHs with various
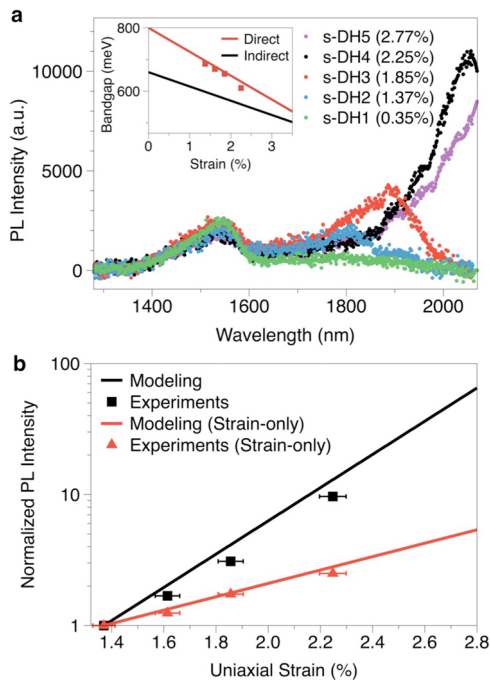

Figure 4. Enhanced and wavelength-shifted light emission from the strain-induced potential wells. (a) PL emission spectra from s-DHs with different strain levels in the active region. The same excitation level is used in all measurements. The inset shows the simulated band gap energies of the direct (red) and the indirect (black) band gaps. Experimental data points represent the measured peak emission energies from the active regions with different strains, and theoretical curves are from deformation potentials. (b) Theoretical PL enhancement with (black) and without (red) the carrier confinement effect. Experimental data points are shown as squares and triangles. Error bars in part b and in the inset to part a represent the root-mean-square (rms) errors between the Lorentzian fitting curves and the measured data.

active region strain levels (the same optical excitation power was used in all cases). The emission from s-DH1 (strain in the active region: 0.35%) exhibits two peaks: one at 1.55 μm from the Ge direct gap transition and the other at 1.8 μm from the Ge indirect gap transition. Both of these peaks correspond mainly to emission from the lightly strained barrier region, as evidenced by the fact that this emission spectrum is identical to that from only the barrier. The emission from the 0.35% strained active region is negligible because the active region has much less area than the barrier and because of significant surface recombination within the nanowire. With such a lightly strained active region, the emission enhancement due to carrier concentration is not strong enough to make the active region emission comparable to the barrier emission. However, as the strain in the active region is increased, emission from it becomes significant while emission from the barrier does not change noticeably. The direct band gap emission from 1.37%, 1.85%, 2.25%, and 2.77% strained active regions corresponds to the long-wavelength peaks of spectra in Figure 4a. The indirect

band gap emission from the strained active regions was not observed because the emission wavelengths were red-shifted beyond the detector cutoff of 2.10 μm due to band gap narrowing. Increasing the strain from 1.37% to 2.25% enhances the direct band gap emission by a factor of 10, while redshifting the peak wavelength to 2.05 μm. The emission spectrum from the 2.77% strained active region is red-shifted beyond the detector cutoff of 2.10 μm, showing only the tail of the spectrum. These experimentally observed redshifts of the emission peak-wavelengths are in good agreement with the predicted strain-induced band gap reductions shown in the inset of Figure 4a.

Figure 4b shows the predicted PL emission enhancement from the active region due to the presence of the strain-induced potential well. For this modeling, the system is approximated as having flat quasi-Fermi levels for its steady state carrier distribution, as shown in Figure 1b. This approximation of flat quasi-Fermi levels is justified if the carrier diffusion length in Ge is longer than the 4.5 μm length of the active region. Pessimistically assuming a minority carrier lifetime in Ge of $\tau \approx$ 10 ns, an order of magnitude less than commonly used,[21] and a carrier diffusion coefficient of $D \approx 50$ cm^2/s,[22] we compute a diffusion length of 7.1 μm. Then, using nondegenerate carrier statistics, a simple relation between band structure and PL emission is obtained in the form of eq 1, derived in detail in the Supporting Information:

$$\text{emission rate} \propto \exp[-E_{g,\Gamma}/kT] \tag{1}$$

where $E_{g,\Gamma}$ is the direct (Γ) band gap energy, k is the Boltzmann constant, and T is the absolute temperature. Squares represent experimentally measured active region emission peak intensities normalized to the emission from the active region of the 1.37% strained s-DH. Our model (solid line) predicts an emission enhancement of 18× for every 1% increase in uniaxial strain with carrier confinement in the s-DHs. This is in good agreement with the experimental fit to the measured data points (squares) presenting an enhancement of 14× for every 1% increase in strain. The slightly smaller measured enhancement compared to the theoretical prediction may be caused by greater surface recombination in the active region.

Since strain alone is also expected to enhance the emission from Ge slightly by reducing the energy difference between the direct and indirect band gaps,[21,23−25] the emission enhancement only by strain is predicted in the form of eq 2, derived in detail in the Supporting Information as well:

$$\text{emission rate} \propto \exp[(E_{c,\Gamma} - E_{c,L})/kT] \tag{2}$$

where $E_{c,\Gamma}$ and $E_{c,L}$ represent the conduction band edges of the direct (Γ) band gap and the indirect (L) band gaps, respectively. As shown in the red solid curve of Figure 4b, strain without the heterostructure effect is expected to enhance emission only by a factor of 3 for every 1% strain, which is also in excellent agreement with the experiments. Experimental data points in red triangles representing the enhancement only due to strain were measured by tightly focusing the optical pumping exclusively onto the active region in order to prevent carriers diffusing in from the barrier (see Figure S5 in the Supporting Information for schematics of band diagrams). Since the total enhancement is 14× per 1% strain, an additional ~5× enhancement for every 1% strain from the pseudo-heterostructure nanowire can be attributed to the carrier confinement effect within the potential well of the active region.

Since the emission from the strain-induced potential well is enhanced exponentially by strain, we infer that ~2.3% strain increases the PL emission from the pseudoheterostructure nanowire by >200× compared to the unstrained case.

In summary, we have created single-material pseudoheterostructure nanowires with custom-designed electronic band profiles by tuning strain profiles at the nanoscale. Strain-induced pseudoheterostructures with potential well depths exceeding kT enabled strong carrier confinement within highly strained nanowires at room temperature. We have experimentally validated this concept by demonstrating spatially confined, enhanced, and wavelength shifted light emission from the nanowires. Although only uniaxial strain along the [100] direction was investigated in this experiment, it should be noted that other directions and types of tensile strain, such as uniaxial strain along the [110] and [111] directions, biaxial strain and hydrostatic strain, can also induce deep and localized potential wells for creating pseudoheterostructures with different deformation potentials.[17]

One immediate application for this work is in double-heterostructure nanolasers, both because of recent interest in Ge lasers[26−28] and because this approach is expected to be very general and should be transferable to III−V materials which have been used extensively as laser gain media.[7,29] The ability to achieve multiple heterostructures with different band gaps on a single die should enable the creation of integrated multiwavelength light sources. This could be as simple as multicolor or white LEDs,[30] or as involved as dense wavelength division multiplexing for optical interconnects by accessing a wide range of band gaps.[31,32] Heterostructure electronics are yet another possibility, for instance serving to achieve high injection velocities from a wide-bandgap region into a narrow-bandgap region in nanowire FETs.[33] At the most general level, the presented approach represents a fundamentally new paradigm for creating nanoscale devices with full heterostructure behavior which previously required multiple semiconductor materials grown on top of each other. It not only reduces the fabrication complexities associated with integrating high-quality layers of different semiconductor materials but also introduces unprecedented design flexibility for creating nanoscale heterostructures.

■ ASSOCIATED CONTENT

Ⓢ Supporting Information

Detailed descriptions of fabrication, measurement, theoretical modeling, and additional figures. This material is available free of charge via the Internet at http://pubs.acs.org.

■ AUTHOR INFORMATION

Corresponding Author

*E-mail: saraswat@stanford.edu and brongersma@stanford.edu.

Notes

The authors declare no competing financial interest.

■ ACKNOWLEDGMENTS

■ REFERENCES

(1) Kroemer, H. *Proc. IEEE* **1963**, *51*, 1782−1783.
(2) Capasso, F.; Luryi, S.; Tsang, W.; Bethea, C.; Levine, B. *Phys. Rev. Lett.* **1983**, *51*, 2318−2321.
(3) Qian, F.; Li, Y.; Gradecak, S.; Park, H.-G.; Dong, Y.; Ding, Y.; Wang, Z. L.; Lieber, C. M. *Nat. Mater.* **2008**, *7*, 701−6.
(4) Polman, A.; Atwater, H. *Nat. Mater.* **2012**, *11*, 174−7.
(5) Wang, X.; Koleilat, G.; Tang, J.; Liu, H. *Nat. Photonics* **2011**, *5*, 480−484.
(6) Hayashi, I.; Panish, M. B.; Foy, P. W.; Sumski, S. *Appl. Phys. Lett.* **1970**, *17*, 109.
(7) Ellis, B.; Mayer, M. A.; Shambat, G.; Sarmiento, T.; Harris, J.; Haller, E. E. *Nat. Photonics* **2011**, *5*, 297−300.
(8) Cho, A. Y. *J. Vac. Sci. Technol.* **1971**, *8*, S31.
(9) Fischetti, M. V.; Laux, S. E. *J. Appl. Phys.* **1996**, *80*, 2234.
(10) Asai, H.; Oe, K. *J. Appl. Phys.* **1983**, *54*, 2052.
(11) Greil, J.; Lugstein, A.; Zeiner, C.; Strasser, G.; Bertagnolli, E. *Nano Lett.* **2012**, *12*, 6230−4.
(12) Signorello, G.; Karg, S.; Björk, M. T.; Gotsmann, B.; Riel, H. *Nano Lett.* **2013**, *13*, 917−24.
(13) Feng, J.; Qian, X.; Huang, C.-W.; Li, J. *Nat. Photonics* **2012**, *6*, 866−872.
(14) Kash, K.; Van der Gaag, B. P.; Mahoney, D. D.; Gozdz, A. S.; Florez, L. T.; Harbison, J. P.; Sturge, M. D. *Phys. Rev. Lett.* **1991**, *67*, 1326−1329.
(15) Huang, M.; Ritz, C. S.; Novakovic, B.; Yu, D.; Zhang, Y.; Flack, F.; Savage, D. E.; Evans, P. G.; Knezevic, I.; Liu, F.; Lagally, M. G. *ACS Nano* **2009**, *3*, 721−727.
(16) Minamisawa, R. A.; Süess, M. J.; Spolenak, R.; Faist, J.; David, C.; Gobrecht, J.; Bourdelle, K. K.; Sigg, H. *Nat. Commun.* **2012**, *3*, 1096.
(17) Van De Walle, C. *Phys. Rev. B* **1989**, *39*, 1871−1883.
(18) Kroemer, H. *RCA Rev.* **1957**, *18*, 332−342.
(19) Tsang, W. T. *Appl. Phys. Lett.* **1982**, *40*, 217.
(20) Chinn, S. R.; Zory, P. S.; Reisinger, A. R. *IEEE J. Quantum Electron.* **1988**, *24*, 2191−2214.
(21) Liu, J.; Sun, X.; Pan, D.; Wang, X.; Kimerling, L. C.; Koch, T. L.; Michel, J. *Opt. Express* **2007**, *15*, 11272−7.
(22) Haynes, J.; Shockley, W. *Phys. Rev.* **1951**, 295.
(23) Nam, D.; Sukhdeo, D.; Roy, A.; Balram, K.; Cheng, S.-L.; Huang, K. C.-Y.; Yuan, Z.; Brongersma, M.; Nishi, Y.; Miller, D.; Saraswat, K. *Opt. Express* **2011**, *19*, 25866−72.
(24) Nam, D.; Sukhdeo, D.; Cheng, S.-L.; Roy, A.; Huang, K. C.-Y.; Brongersma, M.; Nishi, Y.; Saraswat, K. *Appl. Phys. Lett.* **2012**, *100*, 131112.
(25) Sánchez-Pérez, J. R.; Boztug, C.; Chen, F.; Sudradjat, F. F.; Paskiewicz, D. M.; Jacobson, R. B.; Lagally, M. G.; Paiella, R. *Proc. Natl. Acad. Sci.* **2011**, *108*, 18893−8.
(26) Liu, J.; Sun, X.; Camacho-Aguilera, R.; Kimerling, L. C.; Michel, J. *Opt. Lett.* **2010**, *35*, 679−81.
(27) Jain, J. R.; Hryciw, A.; Baer, T. M.; Miller, D. A. B.; Brongersma, M. L.; Howe, R. T. *Nat. Photonics* **2012**, *6*, 398−405.
(28) Camacho-Aguilera, R. E.; Cai, Y.; Patel, N.; Bessette, J. T.; Romagnoli, M.; Kimerling, L. C.; Michel, J. *Opt. Express* **2012**, *20*, 11316−20.
(29) Park, H.-G.; Kim, S.-H.; Kwon, S.-H.; Ju, Y.-G.; Yang, J.-K.; Baek, J.-H.; Kim, S.-B.; Lee, Y.-H. *Science* **2004**, *305*, 1444−7.
(30) Waltereit, P.; Brandt, O.; Trampert, A.; Grahn, H.; Menniger, J.; Ramsteiner, M.; Reiche, M.; Ploog, K. *Nature* **2000**, *406*, 865−8.
(31) Miller, D. *Proc. IEEE* **2009**, *97*, 1166−1185.
(32) Koch, T. L.; Koren, U. *IEEE J. Quantum Electron.* **1991**, *27*, 641−653.

(33) Asbeck, P. M.; Wang, K. C.; Miller, D. L.; Sullivan, G. J.; Sheng, N. H.; Sovero, E. A.; Higgins, J. A. *Microwave Millimeter-Wave Integr. Circuits* **1987**, *83*, 1−5.